PAPER

Check for updates

Impact of catalyst support on water-assisted CO oxidation over PdO/MO$_2$ (M = Sn, Ti, and Si) catalysts: experimental and theoretical investigation†

Kun Liu,*[a] Luliang Liao[b] and Guangfu Liao [iD] *[c]

This study examines the impact of different supports, SnO$_2$, TiO$_2$, and SiO$_2$, on the catalytic performance and water resistance of PdO-based catalysts for CO oxidation. By merging experimental data with DFT calculations, we reveal the distinct characteristics exhibited by each catalyst. Specifically, PdO/TiO$_2$ stands out with exceptional CO oxidation activity, attributed to its minute Pd grain size, robust CO adsorption capacity, and optimal Pd dispersion on the TiO$_2$ surface. In stark contrast, PdO/SnO$_2$ demonstrates heightened activity in the presence of water vapor, whereas PdO/SiO$_2$ experiences minimal effects, as evidenced by quantitative H$_2$O-TPD analysis and DFT simulations of surface interactions. Water vapor exerts differential impacts on the catalytic performance of these catalysts by modulating the energy barriers associated with the CO oxidation mechanisms. On PdO/TiO$_2$, the presence of H$_2$O or H−OH elevates the energy barrier for CO to abstract surface oxygen, thereby diminishing catalyst activity under humid conditions and gradually leading to deactivation due to accumulated surface H$_2$O and OH species. Conversely, on PdO/SnO$_2$, when H$_2$O is present in the form of OH, the energy barrier diminishes, augmenting CO oxidation activity owing to the beneficial effects of surface OH groups.

Introduction

CO oxidation is extensively studied due to its scientific and industrial importance, being crucial for removing CO from exhaust gases and purifying hydrogen in fuel cells.[1–8] As one of the three harmful substances targeted by catalytic converters, CO is typically converted to CO$_2$ through oxidation.[5,9–12] While basic research on gas-phase reactions often uses dry gases, real-world conditions inevitably involve H$_2$O. For applications, under harsher conditions, like vehicle exhaust treatment during startup and catalytic CO removal from flue gas, catalysts must remain active at low temperatures and in the presence of water vapor.[13–20]

In 1977, Fuller *et al.*[21] investigated CO oxidation on PdO/ SnO$_2$ catalysts under humid conditions and discovered that water vapor not only does not poison the catalyst but it significantly enhances its activity. This synergistic effect is due to the

accelerated migration of activated CO from the PdO surface to the SnO$_2$ surface in the presence of water. Conversely, the catalytic efficiency of SnO$_2$ and PdO/SiO$_2$ diminishes under humid conditions. One plausible explanation is that H$_2$O generates hydroxylated sites on the SnO$_2$ surface, which act as chemical bridges facilitating CO spillover activated by PdO. Adsorbed proton acceptors, such as water and alcohols, can aid the transfer of activated hydrogen from the noble metal surface to the oxide surface. However, the precise mechanism by which PdO activates CO prior to spillover remains unclear. Wang *et al.*[22] explored a SnO$_2$-modified PdO/Al$_2$O$_3$ catalyst for CO oxidation, revealing that its activity increases in the presence of H$_2$O and remains stable under prolonged steam conditions. Similarly, Xu *et al.*[23] observed that H$_2$O enhances CO oxidation over PdO/SnO$_2$ catalysts supported by Sn–Al solid solutions. Sun *et al.*[24] demonstrated that Sn-modified Co$_3$O$_4$ catalysts are effective for CO oxidation, with Sn addition significantly inhibiting H$_2$O adsorption and enhancing water resistance. Similarly, Liu *et al.*[25] found that water deactivates Hopcalite catalysts, but SnO$_2$ addition improves their water resistance. Choi *et al.*[26] used theoretical calculations to show that H$_2$O on the PdO (101) surface promotes CO oxidation by stabilizing the carboxyl-like transition state through hydrogen bonding, thus lowering the CO oxidation energy barrier. Despite these findings, the impact of water on PdO-based catalysts and the

[a]School of Resources and Environment, Nanchang University, 999 Xuefu Road, Nanchang, Jiangxi, 330031, China. E-mail: liukun@ncu.edu.cn
[b]Jiangxi Science Technology Normal University, Nanchang, Jiangxi, China
[c]College of Materials Engineering, Fujian Agriculture and Forestry University, Fuzhou 350002, China. E-mail: liaogf@mail2.sysu.edu.cn
†Electronic supplementary information (ESI) available. See DOI: https://doi.org/10.1039/d4nr03963g

mechanisms involved require further systematic study. Additionally, the effect of supports on the water resistance of PdO catalysts is rarely reported. Rutile TiO_2 and SnO_2, with similar crystal structures and cell parameters, are common catalyst supports in heterogeneous catalysis. While PdO/TiO_2 shows good catalytic oxidation performance, studies on the effect of water on PdO/TiO_2 catalysts for CO oxidation are yet to be reported.[27]

The current study investigates the influence of SnO_2, TiO_2 and SiO_2 supports on the catalytic performance and water resistance of PdO-based catalysts for CO oxidation through a combination of experimental results and density functional theory (DFT) calculations. PdO/SnO_2 and PdO/TiO_2 catalysts were synthesized using SnO_2 and rutile-type TiO_2 supports, both sharing the same crystal structure, while PdO/SiO_2 was prepared as a diluent with a similar specific surface area to characterize the intrinsic properties of PdO. Different corresponding catalyst models were constructed while employing a combined theoretical and experimental approach to examine the effect of these supports on CO oxidation activity and water resistance. Our findings reveal that PdO/TiO_2 exhibits superior CO oxidation activity due to optimal Pd dispersion, PdO/SnO_2 shows enhanced activity in the presence of water vapor, and

Guangfu Liao received his PhD degree in Materials Physics & Chemistry from Sun Yat-sen University in 2020. Then he joined the laboratory of Prof. Yi-Chun Lu at the Chinese University of Hong Kong working as a research associate. Subsequently, he was a researcher at the China University of Geosciences. Now, he is a professor in Fujian Agriculture and Forestry University. His research interests

Guangfu Liao

involve photo- and electrocatalysis, polymer synthesis and applications, polymer membranes, nanoporous and nanostructured materials, biomaterials, gas storage and energy conversion, etc. The broader impacts of his research include polymeric photocatalysts, polymer design and synthesis, nanostructure engineering, and biomaterials. So far, he has published more than 80 high profile SCI papers in journals such as Matter, Progress in Materials Science, Energy & Environmental Science, Physics Reports, Applied Catalysis B: Environmental, Nano Energy, ACS Catalysis, Chemical Science, *etc. The awards he has received up to now include the Young Elite Scientists Sponsorship Program by CAST, the 2022* Journal of Materials Chemistry A *Emerging Investigators, the 2023* Chemical Communications *Emerging Investigators, etc. In addition, he also serves on the Youth Editorial Board for* Advanced Fiber Materials, Exploration, eScience, *etc.*
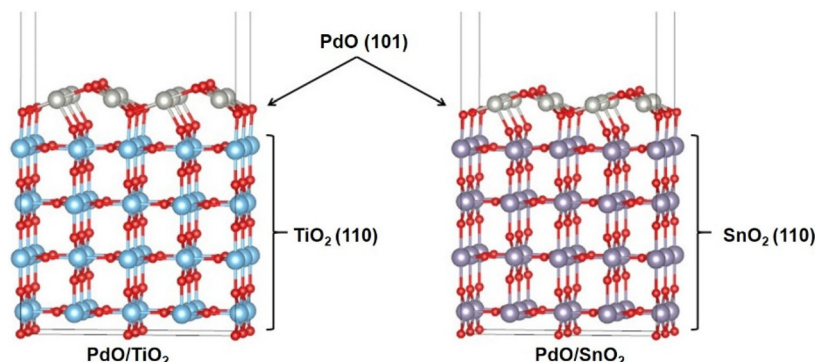
PdO/SiO_2 remains largely unaffected. These results underscore the critical role of catalyst supports in determining CO oxidation efficiency and water tolerance.

Experiment

Methodology and modeling

The quantum chemical calculations in this study were conducted using VASP software with the DFT-D3 method, incorporating van der Waals corrections and spin polarization. PAW–PBE pseudopotentials were used to describe electronic and ionic interactions with a cutoff energy of 400 eV. The k-point grid size ($4 \times 2 \times 1$ or $2 \times 2 \times 1$) was selected based on the cell size and generated using the Monkhorst–Pack method. The convergence criteria were set at 0.01 meV for energy and 0.01 eV $Å^{-1}$ for forces, and a 15 Å vacuum layer with dipole corrections along the z-direction was included. To correct the interactions between Ti 3d electrons, we applied a Hubbard U parameter ($U − J = 4$). The CI-NEB method was used to locate transition states, verified by the single imaginary frequency criterion.

The PdO space group is $P42/mmc$, while SnO_2 and rutile-type TiO_2 belong to the $P42/mnm$ space group, characterized by lattice parameters $a = b \neq c$ and $\alpha = \beta = \gamma = 90°$. The lattice parameters, as listed in Table S1,† align with the experimental values. Sun et al.[28] studied H_2 adsorption and dissociation on n ML PdO supported on TiO_2, finding that the properties of 2–4 ML PdO resemble pure PdO, whereas 1 ML PdO/TiO_2 exhibits unique characteristics. Given the low PdO loading in this study, we used a 1 ML PdO model on TiO_2 and SnO_2 surfaces to form PdO/TiO_2 and PdO/SnO_2 catalyst models. The respective crystallographic planes are as follows: PdO (101) R90 with dimensions 3.058 Å × 6.223 Å, TiO_2 (110) with dimensions 2.990 Å × 6.462 Å, and SnO_2 (110) with dimensions 3.220 Å × 6.740 Å. The PdO (101) R90 and TiO_2 (110) parameters are well matched, whereas PdO (101) R90 and SnO_2 (110) have different parameters; thus, the average cell parameters are used for alignment. A 15 Å vacuum layer was added in the z-direction to prevent interlayer interactions. The specific model is depicted in Fig. 1, where the bottom 9 atomic layers are fixed in the bulk phase, and the others are fully relaxed during calculations.

The adsorption energy is defined as $E_{ads} = E_{adsorbate/substrate} − (E_{adsorbate} + E_{substrate})$, where $E_{adsorbate/substrate}$ is the energy of the entire system after adsorption, $E_{adsorbate}$ is the energy of the adsorbate in its free state, and $E_{substrate}$ represents the energy of the substrate. When the adsorption energy is negative, it indicates an exothermic process.

Results and discussion

The specific surface areas of the catalysts and their supports were measured using the N_2-BET method, as detailed in Table S2.† The supports (SnO_2, TiO_2, SiO_2) demonstrated

Fig. 1 Model diagrams of the PdO/TiO$_2$ and PdO/SnO$_2$ catalysts that were constructed utilizing VASP software by application of the DFT-D3 method.

similar surface areas of 34, 27, and 26 m^2 g^{-1}, respectively, thereby minimizing the influence of the support surface area in the experiments. After loading with PdO, the PdO/SnO$_2$, PdO/TiO$_2$, and PdO/SiO$_2$ catalysts exhibited surface areas of 30, 25 and 25 m^2 g^{-1}, respectively. The X-ray diffraction (XRD) results of these catalysts are presented in Fig. 2. For PdO/SiO$_2$, the broad peak at 21.6° corresponds to SiO$_2$, indicating low crystallinity. The peak at 33.96° observed in both PdO/SiO$_2$ and PdO/TiO$_2$ samples corresponds to the (101) plane of PdO. In PdO/TiO$_2$, peaks corresponding to rutile-type TiO$_2$ were also detected alongside PdO peaks. For PdO/SnO$_2$, peaks at 26.61°, 33.89°, and 51.78° are characteristic of SnO$_2$, with the 33.89° peak coinciding with the PdO (101) peak at 33.96° seen in the PdO/SiO$_2$ and PdO/TiO$_2$ samples, indicating the presence of PdO features in PdO/SnO$_2$. The crystallite sizes of PdO were calculated as 24 nm on SiO$_2$ and 13 nm on TiO$_2$, suggesting better dispersion of PdO on TiO$_2$ surfaces.

Fig. 2 X-ray diffraction (XRD) spectra of both the fresh catalysts and their respective supports.

Catalyst activity testing for CO oxidation and the influence of H$_2$O on CO oxidation performance

The catalyst activity for CO oxidation and the influence of H$_2$O on CO oxidation performance are shown in Fig. 3. Under dry conditions, PdO/TiO$_2$ exhibited the highest catalytic activity, achieving 10% CO conversion at 60 °C and 100% at 130 °C. In contrast, PdO/SiO$_2$ showed the lowest activity, with a T10 (temperature at 10% conversion) of 185 °C and a T100 (temperature for complete conversion) of 210 °C. The catalytic activity for CO oxidation followed the sequence: PdO/TiO$_2$ > PdO/SnO$_2$ > PdO/SiO$_2$.

In the presence of water vapor, the CO oxidation activity of PdO/TiO$_2$ decreased significantly, with T10 increasing to 90 °C and achieving 100% conversion at 140 °C. Conversely, under dry conditions, the CO oxidation activity of PdO/SnO$_2$ increased, with T10 decreasing from 115 °C to 100 °C, and the complete conversion temperature reducing from 140 °C to 130 °C. For PdO/SiO$_2$, the CO oxidation activity slightly decreased at lower temperatures (T10 increased from 185 °C to 195 °C) under wet conditions, but showed no significant change at higher temperatures. Table S3† presents a quantitative analysis of the surface CO oxidation reactivity of various catalysts, focusing on their apparent activation energy (E_a) and reaction rates at 100 °C, derived using Arrhenius plots. Under anhydrous conditions, the E_a values for surface CO oxidation increased in the order: PdO/TiO$_2$ > PdO/SnO$_2$ > PdO/SiO$_2$, consistent with their reaction activity. In the presence of water, the E_a value for PdO/TiO$_2$ increased by 8.77 kJ mol^{-1}, while for PdO/SnO$_2$ it decreased by 8.31 kJ mol^{-1}, correlating with the changes in catalytic activity. Additionally, normalized reaction rates (R_w) for low conversions (<20%) by catalyst mass showed R_w values in the sequence: PdO/TiO$_2$ > PdO/SnO$_2$ > PdO/SiO$_2$, consistent with their activity levels. Fig. 4a shows the stability test results of the PdO/SnO$_2$ catalyst for CO oxidation at 110 °C under humid conditions. At 110 °C without water, the CO conversion rate is around 10%, which increases to about 90% stable for 30 hours in the presence of water. Furthermore, the catalyst activity remains stable after water removal, showcasing the PdO/SnO$_2$ catalyst's enhanced CO oxidation activity and its potential for water-resistant applications.
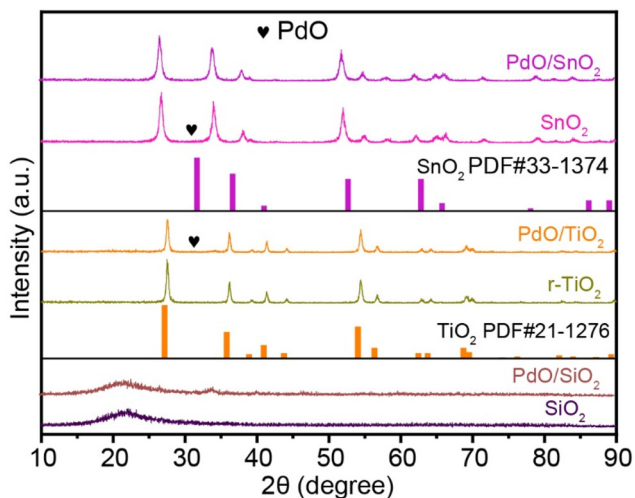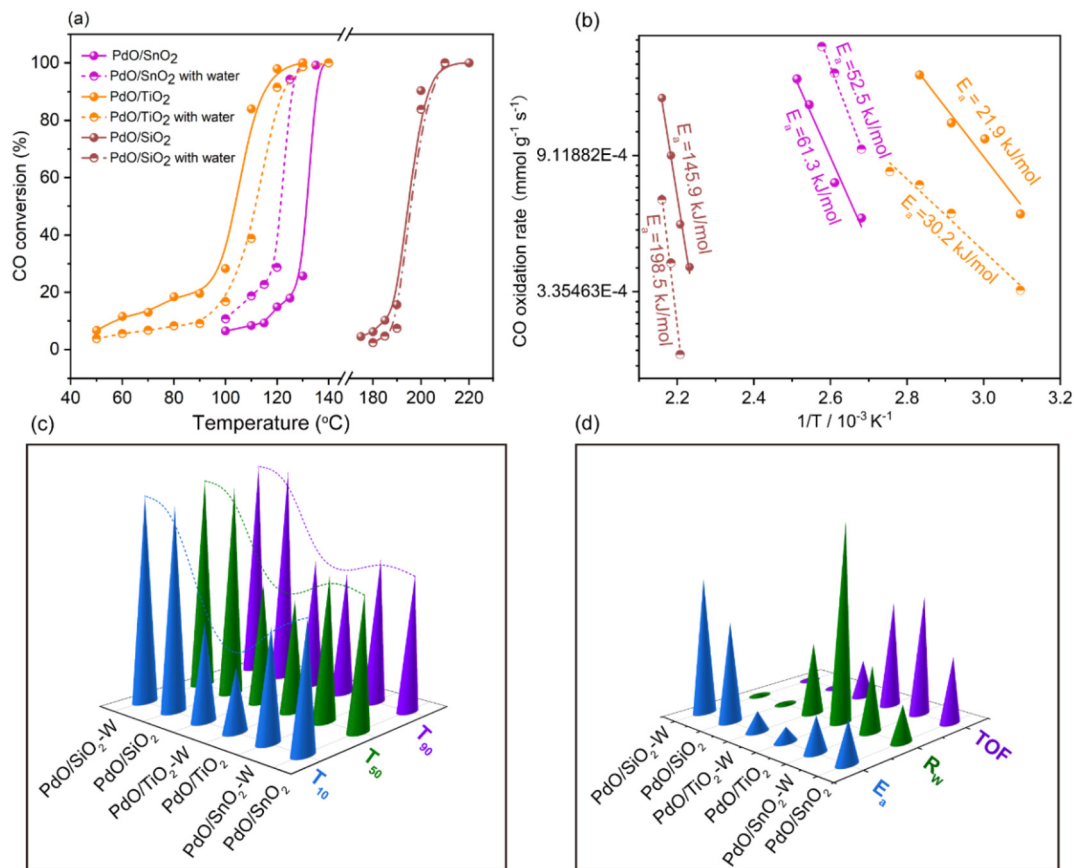
Fig. 3 (a) CO conversion rate *vs.* temperature curve; (b) Arrhenius plot for catalyst surface CO oxidation activity of PdO/TiO$_2$-W, where "W" refers to water. Reaction conditions: 1 bar, with a weight hourly space velocity (WHSV) of 72 000 mL g^{-1} h^{-1}. (c) The corresponding reaction temperatures for all catalysts at T$_{10}$, T$_{50}$, and T$_{90}$ (Note: T$_{10}$ represents the reaction temperature corresponding to a 10% CO conversion rate for the catalyst). (d) The intrinsic reaction performance parameters for all catalysts (E_a: activation energy; R_w: intrinsic reactivity per unit mass of the catalyst; TOF: turnover frequency).

Fig. 4b shows that at a reaction temperature of 110 °C for the PdO/TiO$_2$ catalyst, the CO oxidation conversion rate is around 95%, which gradually decreases to about 20% over 20 hours and then stabilizes in the presence of water. Meanwhile, upon removing the water, the activity immediately returns to the dry condition level of a stable high conversion rate (90%), illustrating the poor water resistance behavior of the PdO/TiO$_2$ catalyst, where water can reversibly affect the CO oxidation process. For the PdO/SiO$_2$ catalyst shown in Fig. 4c, the CO conversion rate can be noticed at around 95% at 190 °C, while fluctuating between 88% and 95% in the presence of water, with no significant decline in activity over 30 hours. This indicates that water has no impact on the catalyst's activity, and the catalyst exhibits water resistance during CO oxidation. Further investigations were carried out using XPS, TPR and TPD characterization studies to elucidate the different CO oxidation activity trends and stability characteristics of these catalysts under wet conditions.

Analysis of the surface composition and H$_2$O and CO adsorption properties on catalyst surfaces by different characterization approaches

The surface properties of the catalysts were investigated by XPS, with the results shown in Fig. 5 and Table S4.† The Pd3d

spectra revealed peaks at 336.6 and 342.0 eV corresponding to Pd^{2+}, indicating that Pd species on the surface of all three catalysts exist as Pd^{2+}. The quantitative results listed in Table S4† illustrate that the PdO/TiO$_2$ catalyst boasts the highest surface Pd content of 4.76 wt%, followed by PdO/SnO$_2$ with 2.31 wt% and PdO/SiO$_2$ with 1.08 wt%. However, the ICP results showed that the bulk Pd content was similar across the three catalysts, with PdO/TiO$_2$, PdO/SnO$_2$, and PdO/SiO$_2$ containing 1.69, 1.64 and 1.75 wt% Pd, respectively. These observations suggest that TiO$_2$ enhances Pd dispersion more effectively, a conclusion supported by XRD grain size measurements. The CO-TPD results (Table S4†) also indicated that surface Pd dispersion follows the order PdO/TiO$_2$ > PdO/SnO$_2$ > PdO/SiO$_2$, underscoring the critical role of Pd dispersion in the performance of PdO-based catalysts. Meanwhile for the deconvolution of the O 1s peaks in PdO/TiO$_2$ samples, the binding energy at 529.3 eV can be attributed to surface lattice oxygen (O$_{latt}$), and the peaks at 530.1 eV and 531.5 eV can be assigned to surface adsorbed oxygen (O$_{ads}$).[29] In the PdO/SnO$_2$ samples, the binding energies are shifted to 530.5 eV and 531.8 eV, corresponding to O$_{latt}$ and O$_{ads}$, respectively, which further deviate to 531.9 eV (O$_{latt}$) and 532.8 eV (O$_{ads}$) for the PdO/SiO$_2$ catalyst.[30] The quantitative analysis of surface oxygen species (listed in
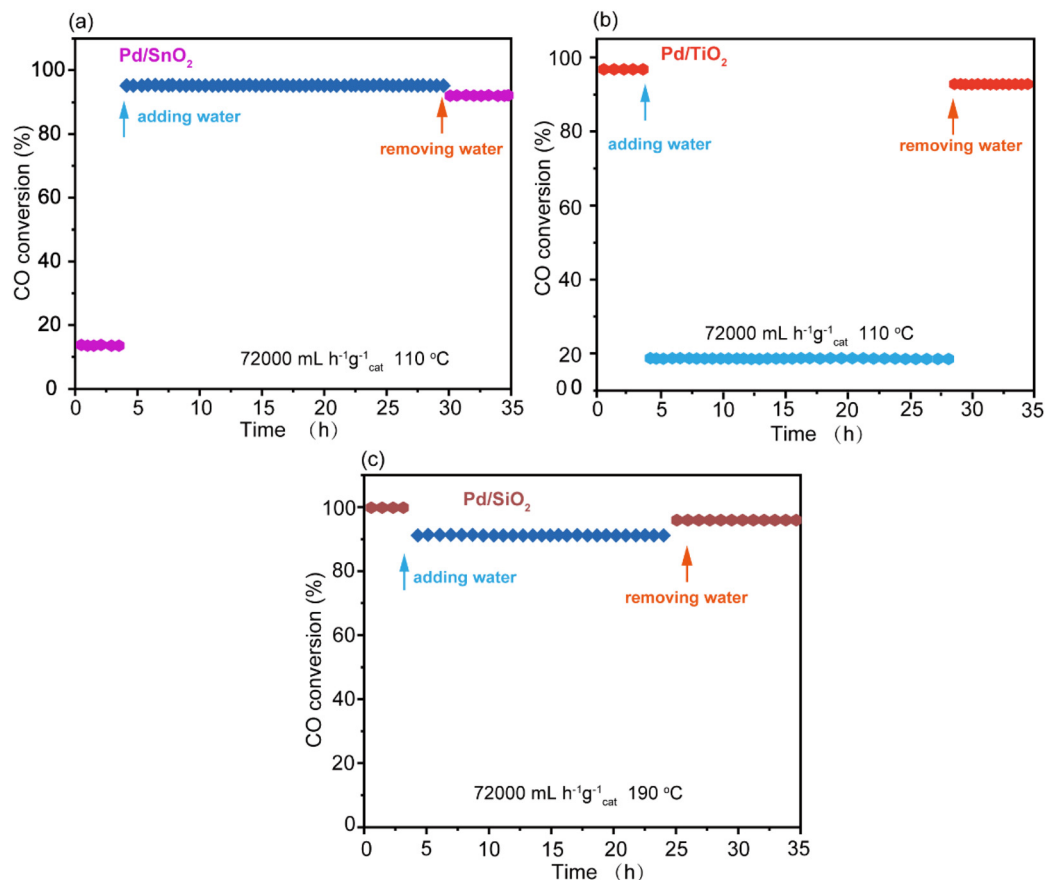
Fig. 4 Stability test of the CO oxidation reaction on catalyst surfaces in the presence of H_2O: (a) Pd/SnO_2, (b) Pd/TiO_2, and (c) Pd/SiO_2. Reaction conditions: 1 bar, with a weight hourly space velocity (WHSV) of 72 000 mL g^{-1} h^{-1}.

Table S4†) showing the $O_{ads}/(O_{ads} + O_{latt})$ ratio of PdO/SiO_2 samples follows the sequence of $PdO/TiO_2 > PdO/SnO_2 > PdO/SiO_2$. This sequence matching the catalytic activity for CO oxidation demonstrates that the amount of surface adsorbed oxygen is another factor influencing catalytic activity.

To study the effects of various supports on PdO, H_2-TPR tests were conducted. The redox properties of the three samples were analyzed by H_2-TPR techniques, with the results shown in Fig. 6a. All three samples exhibit an H_2 desorption peak below 100 °C, which is attributed to hydrogen adsorption on the reduced Pd species. Additionally, the hydrogen spillover effect causes the H_2 consumption peak temperature of SnO_2 to shift to a lower position, while the TiO_2 and SiO_2 supports do not show any reduction peaks. This indicates that PdO maintains strong metal–support interactions with SnO_2, TiO_2, and SiO_2 supports. Three catalysts were tested for water adsorption through H_2O-TPD. The results in Fig. 6b show that PdO/SiO_2 has minimal water adsorption, whereas PdO/TiO_2 and PdO/SnO_2 exhibit significant adsorption. The distinct desorption peaks below and above ~170 °C correspond to water and OH desorption behaviors, respectively.[25] Table S5† provides a quantitative analysis of the desorbed water peak areas across different temperature ranges. The comparative analysis of different peaks highlights that PdO/SnO_2 and PdO/TiO_2 have significant H_2O desorption peaks, unlike PdO/SiO_2, which shows only a minimal peak, illustrating the unchanged catalytic activity of PdO/SiO_2 under both hydrated and dehydrated conditions during CO oxidation. Conversely, PdO/SnO_2 and PdO/TiO_2 exhibit similar large water adsorption capacities with both H_2O and OH surface adsorption, yet display different trends in CO oxidation activity, suggesting the need for further investigation to understand the specific reasons. The CO-TPD spectra (Fig. 6c) and quantitative results (Table S5,† based on integrated desorption peak areas) suggest that PdO/TiO_2 favors the highest CO adsorption behavior with the following order $PdO/TiO_2 > PdO/SnO_2 > PdO/SiO_2$ correlating with a CO oxidation activity sequence. However, a different behavior observed in the presence of water, where PdO/TiO_2 activity decreases, PdO/SnO_2 increases, and PdO/SiO_2 remains consistent, highlights a different scenario. The ambiguous underlying reasons for support and water effects on catalyst activity prompt the construction of a catalyst model for quantum chemical calculations to elucidate the support effects on CO oxidation in the presence of H_2O.

Discussion of DFT calculation results

Adsorption energies of CO, H_2O, and OH on catalyst and support surfaces. Theoretical calculations were used to discuss the catalytic CO oxidation process under two different con-
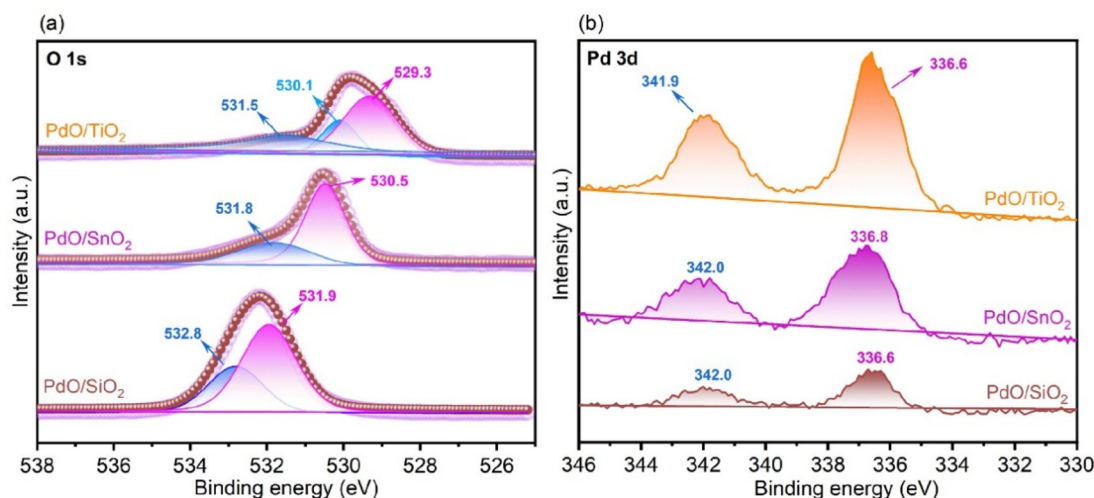
Fig. 5 The XPS spectra of all freshly prepared catalysts are presented as follows: (a) O 1s and (b) Pd 3d XPS spectra of PdO/TiO$_2$, PdO/SnO$_2$, and PdO/SiO$_2$.
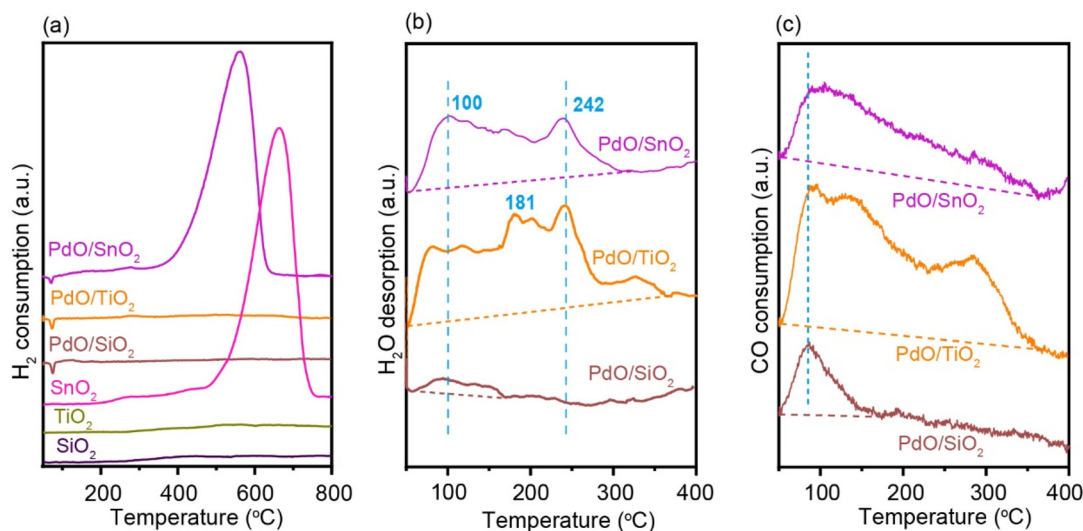

Fig. 6 Characterization of (a) H$_2$O-TPR, (b) H$_2$O-TPD and (c) CO-TPD of all catalysts.

ditions (with and without water). Initially, adsorption of small molecules (CO, H$_2$O, OH) on both catalyst and support surfaces was explored. According to the calculations in Table S6,† the TiO$_2$ support exhibits higher adsorption energy for H$_2$O compared to SnO$_2$, while the adsorption energies of water on the catalyst surfaces decreased upon PdO loading, being consistent with earlier H$_2$O-TPD results. However, on the SnO$_2$ surface, the barrier for H$_2$O dissociation is negative, indicating facile dissociation of water on SnO$_2$. Meanwhile, the TiO$_2$ surface also shows low barriers for H$_2$O dissociation, suggesting that water primarily exists in the OH state on the support surface. After PdO loading, the dissociation barrier of H$_2$O increases slightly, but the barrier for the reverse reaction to form water remains low. Therefore, water exists in both H$_2$O and OH states on the catalyst surface after loading. CO prefers

to adsorb at the top sites of Pd atoms on pure PdO surfaces, while the optimal adsorption position for CO shifts to Pd–O bridge sites on PdO/TiO$_2$ and PdO/SnO$_2$ surfaces.[31] The adsorption energies of CO, H$_2$O, and OH on PdO, PdO/TiO$_2$, and PdO/SnO$_2$ surfaces (Fig. 7a) show that the presence of TiO$_2$ or SnO$_2$ as a support increases the adsorption energies of small molecules. Fig. 7b shows the changes in CO adsorption energy on clean surfaces, surfaces with adsorbed H$_2$O, and surfaces with adsorbed H–OH for various catalysts. It can be observed that the CO adsorption energy increases on PdO/TiO$_2$ and PdO/SnO$_2$ surfaces with pre-adsorbed H$_2$O compared to clean surfaces, indicating that H$_2$O pre-adsorption enhances CO adsorption. However, pre-adsorbed H–OH has no significant effect on the CO adsorption energy on these catalyst surfaces. In contrast, the CO adsorption energy slightly decreases
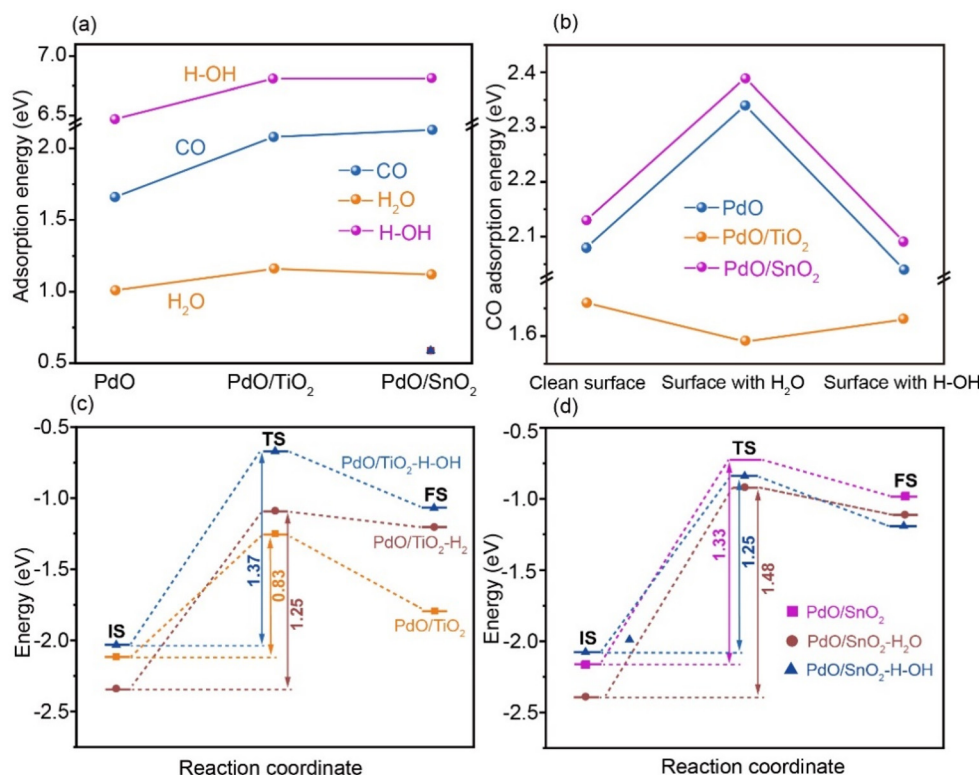
Fig. 7 (a) Adsorption of small molecules on catalyst surfaces, (b) CO adsorption on catalyst surfaces under different conditions, (c) PdO/TiO$_2$ and (d) PdO/SnO$_2$, and the potential energy diagram for CO oxidation on the surface of catalysts.

with pre-adsorbed H$_2$O or H–OH on pure PdO surfaces, suggesting minimal impact of H$_2$O and H–OH on CO adsorption on pure PdO.

The impact of H$_2$O on CO adsorption structures and charge transfer. An interesting phenomenon has been observed in the presence of H$_2$O and its dissociated state H–OH that does not significantly affect CO adsorption on the pure PdO surface. CO prefers to be adsorbed at the Pd$_{top}$ site with similar adsorption energies of 1.66 eV, 1.59 eV, and 1.63 eV, respectively. The C–O bond length remains approximately 1.150 Å, slightly longer than the free molecule length of 1.144 Å, indicating weak substrate activation of CO and minimal charge transfer between CO and the substrate. Analysis of the C–O bond length variation and Bader charge suggests that on the pure PdO surface at the Pd$_{top}$ site, the substrate has a negligible activation effect on CO. On the PdO/TiO$_2$ surface, CO adsorbs on Pd–O bridge sites with an adsorption energy of 2.08 eV, higher than on pure PdO surfaces. As shown in Fig. 8a, the C–O bond length is 1.227 Å, longer than the C–O bond length on pure PdO surfaces (1.150 Å). Bader charge analysis indicates that CO loses 0.48 e upon adsorption, with the lost electrons primarily accumulating on Pd$_{cus}$ and O$_{cus}$, gaining 0.18 e and 0.29 e, respectively. Compared to pure PdO surfaces, the PdO/TiO$_2$ surface exhibits stronger interactions with CO, facilitating CO activation. However, the adsorption energy of CO increases to 2.34 eV (Fig. 8) on the PdO/TiO$_2$ surface in the presence of H$_2$O. The

C–O bond length slightly elongates to 1.241 Å compared to the absence of H$_2$O, indicating the presence of hydrogen bonding between CO and surface H$_2$O, with an O to H distance of 1.795 Å, which enhances the interaction between CO and the surface. Meanwhile, the adsorption energy (2.05 eV) and bond length (1.224 Å) of CO show no significant change compared to the clean surface (Fig. 8c) upon the dissociation of H$_2$O into H–OH on the surface, suggesting that H–OH has little effect on CO adsorption after dissociation. On the other hand, CO preferably adsorbs at Pd–O bridge sites with an adsorption energy of 2.13 eV on the PdO/SnO$_2$ surface (Fig. 9a), which is similar to CO adsorption on the PdO/TiO$_2$ surface. The C–O bond length is 1.228 Å, identical to that on PdO/TiO$_2$ and longer than that on pure PdO surfaces (1.150 Å). Bader charge analysis indicates that the CO molecule loses 0.50 e, predominantly localized on Pd$_{cus}$ and O$_{cus}$ with gains of 0.19 e and 0.31 e, respectively. These results are comparable to those for CO adsorption on PdO/TiO$_2$ surfaces. However, the adsorption energy of CO increases to 2.39 eV in the presence of H$_2$O (Fig. 9b) on the PdO/SnO$_2$ surface, where the C–O bond length extends slightly to 1.246 Å compared to in the absence of H$_2$O. The distance of 1.807 Å between O in CO and H in H$_2$O suggests the presence of hydrogen bonding, strengthening the interaction between CO and the surface. Furthermore, the adsorption energy (2.09 eV) and bond length (1.226 Å) of CO remain unchanged (Fig. 9c) when H$_2$O dissociates into H–OH on the surface compared to adsorption on
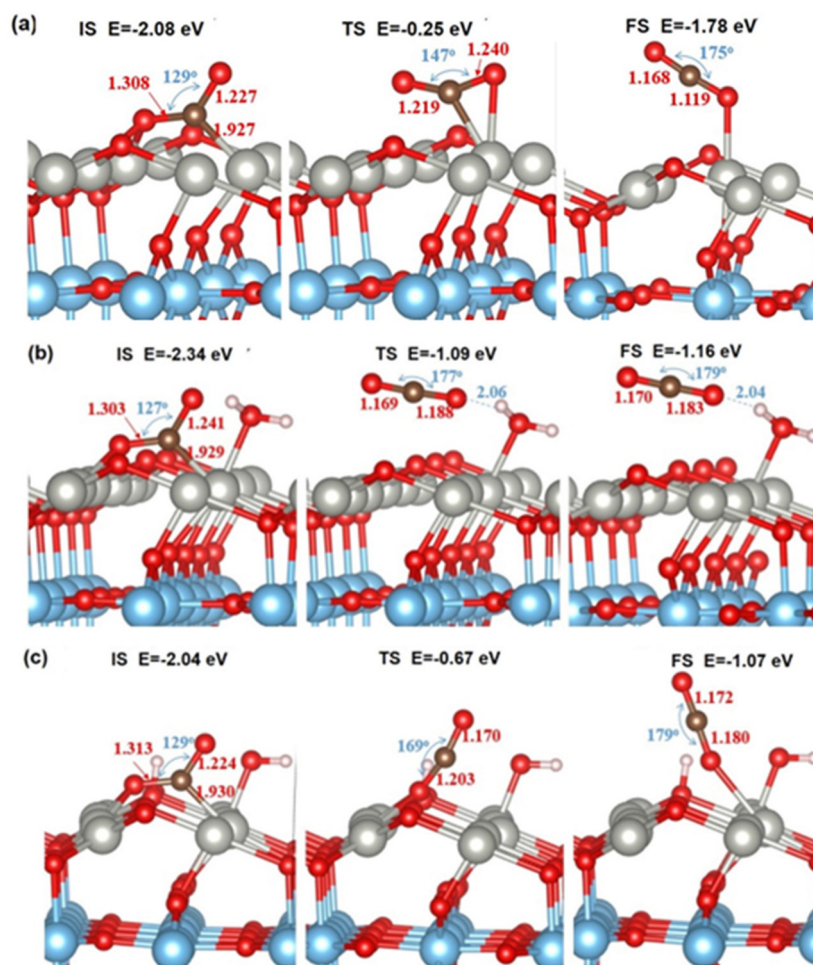
Fig. 8 Surface CO oxidation configuration of PdO/TiO$_2$ in the absence and presence of water. The energy parameters for the (a) initial (IS), (b) transition (TS), and (c) final states (FS) of the catalyst configuration.

the clean surface, indicating that H–OH formation post-dissociation of H$_2$O has a minimal impact on CO adsorption.

The effect of H$_2$O on the oxidation process of CO. In the course of this work, the surface CO oxidation on catalysts follows the Mars–van Krevelen mechanism. Initially, CO molecules adsorb on the catalyst surface, followed by reaction with surface O species to form CO$_2$ and create oxygen vacancies. Oxygen molecules from the air diffuse to the catalyst surface to fill these vacancies, generating active oxygen atoms that react with another CO molecule to form CO$_2$. Simultaneously, the catalyst is regenerated, and the reaction proceeds in a cyclic manner. Fig. 7c, d, 8 and 9 depict the pathway and potential energy diagrams of CO oxidation on the PdO/TiO$_2$ and PdO/SnO$_2$ catalyst surfaces. Energy changes during the reaction are presented in Table S8.†

Fig. 8a indicates that CO initially adsorbs at the Pd–O bridge site while releasing 2.08 eV of energy on the clean PdO/TiO$_2$ catalyst surface. The C–O bond lengthens from the free molecule length of 1.144 Å to 1.227 Å, activating the CO molecule. The activated CO forms an O$_{cus}$–C–O species with surface coordinatively unsaturated O (O$_{cus}$), ultimately extracting the surface O$_{cus}$ to generate the CO$_2$* species, as illustrated in Fig. 7c. This process

requires overcoming an energy barrier of 0.83 eV. In the transition state structure (Fig. 8a), the O$_{cus}$–C–O species initially breaks the Pd–O$_{cus}$ bond to form the adsorbed CO$_2$* species. The bond length of O$_{cus}$–C shortens from its initial adsorption length of 1.308 Å to 1.219 Å, indicating enhanced interaction between C and O$_{cus}$. The generated CO$_2$* species exhibits C–O bond lengths of 1.168 Å and 1.119 Å, with an O–C–O angle of 175°. In contrast, the C–O bond length in a free CO$_2$ molecule is 1.177 Å, with an O–C–O angle of 180°, highlighting the weaker adsorption of CO$_2$ on the catalyst surface compared to its free form. On the surface of the PdO/TiO$_2$ catalyst in the presence of H$_2$O, as depicted in Fig. 8b, CO initially adsorbs at Pd–O bridge sites, releasing 2.34 eV of energy. The C–O bond lengthens from its molecular length of 1.144 Å to 1.241 Å, activating the CO molecule. Activated CO then reacts with surface O$_{cus}$ to form O$_{cus}$–C–O species, eventually departing from the surface as CO$_2$* species. This process requires a barrier of 1.25 eV to be overcome (Fig. 7c).

In the transition state structure, CO is oxidized with surface O$_{cus}$ to form a bent O$_{cus}$–C–O species, where the O$_{cus}$–O bond length shortens from the initial 1.308 Å upon adsorption to 1.169 Å, approaching the C–O bond length in CO$_2$ molecules.
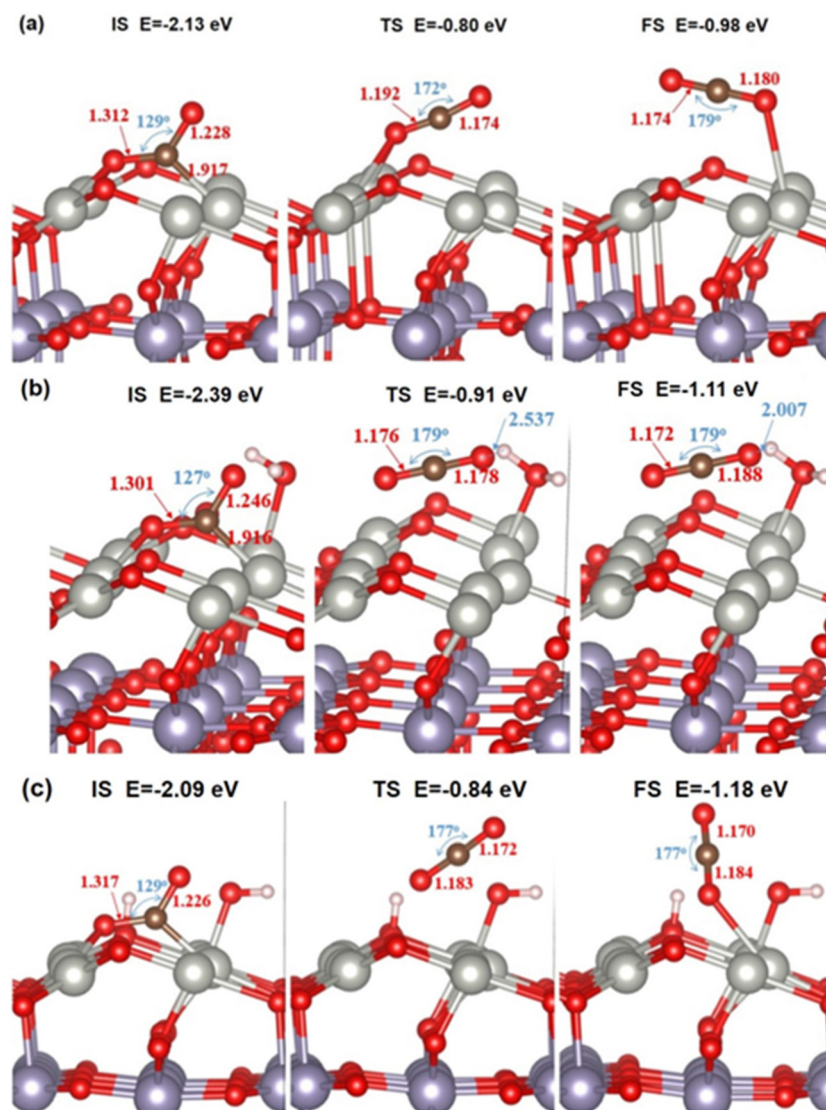
Fig. 9 Surface configuration of the PdO/SnO$_2$ catalyst for CO oxidation under dry and wet conditions The energy parameters for the (a) initial (IS), (b) transition (TS), and (c) final states (FS) of the catalyst configuration.

The generated CO$_2$* species exhibit C–O bond lengths of 1.170 Å and 1.183 Å, with an O–C–O angle of 179°. These results indicate that the presence of H$_2$O impedes the process of CO oxidation with surface O$_{cus}$. In the presence of H–OH on the PdO/TiO$_2$ surface in dissociative form, as shown in Fig. 8c, CO adsorption at Pd–O bridge sites releases 2.04 eV of energy, which is similar to the energy released during CO adsorption on a clean PdO/TiO$_2$ surface. The process of CO oxidation with surface O requires an energy barrier of 1.37 eV to be overcome. In the transition state structure (Fig. 8a), the O$_{cus}$–C–O species initially breaks the Pd$_{cus}$–C bond to form the adsorbed CO$_2$* species. The bond length of O$_{cus}$–C changes from 1.313 Å upon adsorption to 1.203 Å, and the resulting CO$_2$* species has C–O bond lengths of 1.172 and 1.180 Å, with an ∠O–C–O angle of 179°. When H$_2$O is present in the dissociated form H–OH on the PdO/TiO$_2$ surface, as shown in Fig. 8c, CO adsorption on Pd–O bridge sites releases

2.04 eV of energy, which is similar to the energy released when CO adsorbs on a clean PdO/TiO$_2$ surface. The process of CO oxidation with surface O involves overcoming a barrier of 1.37 eV. In the transition state structure (Fig. 8a), the O$_{cus}$–C–O species initially breaks the Pd$_{cus}$–C bond to form the adsorbed CO$_2$* species, with the bond length of O$_{cus}$–C changing from 1.313 Å upon adsorption to 1.203 Å. The resulting CO$_2$* species has C–O bond lengths of 1.172 and 1.180 Å, and an O–C–O angle of 179°. The presence of H–OH alters the bond-breaking process during CO oxidation with surface O, leading to an increased reaction barrier. This indicates that the presence of H–OH further impedes the process of CO oxidation with surface oxygen, which aligns with experimental observations where the presence of H$_2$O reduces CO oxidation activity.

On the PdO/SnO$_2$ catalyst surface, the process of CO oxidation with surface oxygen is illustrated in Fig. 9a–c, with

corresponding changes in potential energy shown in Fig. 7d and Table S8.† The initial and final states of CO during oxygen extraction exhibit structures nearly identical to those on the PdO/TiO_2 surface. However, on the PdO/SnO_2 surface, during the transition state formation of the CO_2* species where CO is oxidized with surface oxygen, the O_{cus}–C–O species breaks the Pd_{cus}–C bond rather than the Pd–O_{cus} bond. The breaking of the Pd_{cus}–C bond is a dynamically more challenging process, resulting in a higher energy barrier for CO oxidation compared to the PdO/TiO_2 surface. When surface H_2O exists in molecular form, the energy barrier for CO oxidation with oxygen is 1.48 eV with an adsorption energy of 1.28 eV. However, when H_2O is in the dissociated form H–OH, the energy barrier decreases to 1.25 eV with an adsorption energy of 0.91 eV. This lower barrier and reduced adsorption energy compared to the clean surface and molecular H_2O conditions indicate that on the PdO/SnO_2 catalyst surface, the enhanced activity in CO oxidation with H_2O primarily stems from the presence of OH species. Moreover, this process is more favorable both kinetically and thermodynamically.

Impact of PdO/MO_2 catalyst support on the CO oxidation reaction under anhydrous and aqueous conditions. In the absence of water during the CO oxidation process, the catalytic activities follow the order PdO/TiO_2 > PdO/SnO_2 > PdO/SiO_2. Characterization results by BET, XRD, TPD, ICP, *etc.* indicate that when catalysts have similar specific surface areas and identical Pd content, the superior CO oxidation activity of PdO/TiO_2 is attributed to the highest dispersion of Pd species on TiO_2. This results in the maximum CO adsorption capacity and surface oxygen content on the catalyst. Compared to PdO/SnO_2, the difference in dispersion between PdO/TiO_2 and SnO_2 may arise from the mismatch in crystal lattice parameters between PdO and TiO_2 or SnO_2. According to Table S1,† PdO (101) exhibits a closer match with the TiO_2 (110) surface lattice parameters upon 90° rotation. Additionally, DFT calculations show that the energy barrier for CO oxidation with surface oxygen is higher on the PdO/SnO_2 surface compared to PdO/TiO_2 during the CO oxidation process, consistent with experimental observations. When water is introduced into the system, the activity of three different catalysts exhibits various changes. The activity of PdO/TiO_2 for CO oxidation decreases, whereas that of PdO/SnO_2 increases. PdO/SiO_2, on the other hand, shows a relatively slight change in activity. The H_2O-TPD results indicate that PdO/SiO_2 adsorbs minimal amounts of water, while PdO/TiO_2 and PdO/SnO_2 exhibit significant water adsorption, with concurrent desorption of both H_2O and OH species. Stability tests reveal that the activity of PdO/TiO_2 for CO oxidation decreases over time upon water addition, stabilizing at around 20% and recovering upon water removal. Conversely, PdO/SnO_2 shows a substantial increase in activity upon water addition, maintaining stability, with no change upon water removal, suggesting a permanent promotional effect of water. Meanwhile, PdO/SiO_2 demonstrates nearly unchanged CO oxidation activity with water addition. The DFT calculations indicate that the dissociation barriers of H_2O are low on both the TiO_2 and SnO_2 supports as well as on the PdO/TiO_2 and PdO/SnO_2 catalysts, allowing the coexistence of H_2O and dissociated H–OH on these surfaces. Introducing H_2O in the PdO/TiO_2 and PdO/SnO_2 systems increases the adsorption energy of CO molecules and raises the reaction barrier for CO oxidation with surface O, indicating that CO activation requires a moderately strong adsorption energy. However, an excessive increase in adsorption energy hinders further CO reaction. In the presence of OH species, the oxidation barrier of CO on PdO/TiO_2 surfaces further increases. Conversely, on PdO/SnO_2 surfaces, the oxidation barrier of CO decreases, accompanied by a reduced exothermic reaction, suggesting that the presence of OH favors CO oxidation on PdO/SnO_2 surfaces both kinetically and thermodynamically.

Conclusion

This work combines experimental and density functional theory (DFT) calculations to investigate the support effects of PdO/MO_2 (M = Sn, Ti, and Si) catalysts on CO oxidation and the impact of the presence of water on their catalytic performance. As the active component, PdO shows different catalytic activities for CO oxidation when supported on TiO_2, SnO_2 and SiO_2 supports, with the activity order: PdO/TiO_2 > PdO/SnO_2 > PdO/SiO_2. PdO/TiO_2 exhibits the smallest Pd grain size, the highest CO adsorption capacity, the maximum surface oxygen content, and the highest Pd dispersion on TiO_2, resulting in superior CO oxidation activity. DFT calculations show that the energy barrier for CO oxidation with surface oxygen is the lowest for PdO/TiO_2, consistent with experimental observations. Upon introducing H_2O into the reaction system, the activity of PdO/TiO_2 decreases, while that of PdO/SnO_2 increases, and PdO/SiO_2 activity remains nearly unchanged. Quantitative results from H_2O-TPD indicate minimal H_2O adsorption on PdO/SiO_2 and significant adsorption on PdO/TiO_2 and PdO/SnO_2, with varying strengths for H_2O and OH adsorption. This explains why H_2O has a minimal impact on PdO/SiO_2 but significant effects on PdO/TiO_2 and PdO/SnO_2 activities. DFT calculations reveal that the presence of H_2O or H–OH species on the surface of PdO/TiO_2 increases the energy barrier for CO oxidation with surface oxygen, leading to reduced activity under wet conditions and eventual deactivation under a humid atmosphere, attributed to the combined effect of surface H_2O and OH. Conversely, on PdO/SnO_2 surfaces, when H_2O exists in the OH state, the energy barrier for CO oxidation with surface oxygen decreases, indicating enhanced CO oxidation activity due to the role of surface OH species.

Author contributions

Kun Liu: investigation, formal analysis, and writing – review & editing. Luliang Liao: investigation. Guangfu Liao: conceptualization and supervision.

Data availability

All the data for this article are available in the main text and the ESI† or upon reasonable request from the corresponding author.

Conflicts of interest

The authors declare that they have no known competing financial interests or personal relationships that could have appeared to influence the work reported in this paper.

Acknowledgements

References

1 G. Liao, J. Fang, Q. Li, S. Li, Z. Xu and B. Fang, *Nanoscale*, 2019, **11**, 7062–7096.

2 S. Lu, S. Zhang, Q. Liu, W. Wang, N. Hao, Y. Wang, Z. Li and D. Luo, *Carbon Neutralization*, 2024, **3**, 142–168.

3 A. Naitabdi, A. Boucly, F. Rochet, R. Fagiewicz, G. Olivieri, F. Bournel, R. Benbalagh, F. Sirotti and J.-J. Gallet, *Nanoscale*, 2018, **10**, 6566–6580.

4 G. Liao, Y. He, H. Wang, B. Fang, N. Tsubaki and C. Li, *Device*, 2023, **1**, 100173.

5 L. Huang, X. Song, Y. Lin, C. Liu, W. He, S. Wang, Z. Long and Z. Sun, *Nanoscale*, 2020, **12**, 3273–3283.

6 G. Liao, G. Ding, B. Yang and C. Li, *Precis. Chem.*, 2024, **2**, 49–56.

7 G. Ding, C. Li, L. Chen and G. Liao, *Energy Environ. Sci.*, 2024, **17**, 5311–5335.

8 G. Ding, C. Li, Y. Ni, L. Chen, L. Shuai and G. Liao, *EES Catal.*, 2023, **1**, 369–391.

9 M. P. Salinas-Quezada, J. K. Pedersen, P. Sebastián-Pascual, I. Chorkendorff, K. Biswas, J. Rossmeisl and M. Escudero-Escribano, *EES Catal.*, 2024, **2**, 941–952.

10 M. Chatterjee, N. Hiyoshi, T. Fukuda and N. Mimura, *Sustainable Energy Fuels*, 2023, **7**, 1878–1892.

11 H. Zhu, W. Qiu, R. Wu, K. Li and H. He, *Catal. Sci. Technol.*, 2024, **14**, 3050–3063.

12 Y. Zhao, G. Chen, N. Zheng and G. Fu, *Faraday Discuss.*, 2014, **176**, 381–392.

13 J. Cai, Z. Liu, K. Cao, Y. Lang, S. Chu, B. Shan and R. Chen, *J. Mater. Chem. A*, 2020, **8**, 10180–10187.

14 Y. Li and W. Shen, *Chem. Soc. Rev.*, 2014, **43**, 1543–1574.

15 X. Liu, Y. Tang, M. Shen, W. Li, S. Chu, B. Shan and R. Chen, *Chem. Sci.*, 2018, **9**, 2469–2473.

16 Y. Liao, K. Wang, G. Liao, M. A. Nawaz and K. Liu, *Catal. Sci. Technol.*, 2024, DOI: **10.1039/D4CY00679H**.

17 H. Zhu, L. Gou, C. Li, X. Fu, Y. Weng, L. Chen, B. Fang, L. Shuai and G. Liao, *Device*, 2024, **2**, 100283.

18 F. Tian, X. Wu, J. Chen, X. Sun, X. Yan and G. Liao, *Dalton Trans.*, 2023, **52**, 11934–11940.

19 J. P. N. Kembo, J. Wang, N. Luo, F. Gao, H. Yi, S. Zhao, Y. Zhou and X. Tang, *New J. Chem.*, 2023, **47**, 20222–20247.

20 G. Liao, C. Li, S.-Y. Liu, B. Fang and H. Yang, *Phys. Rep.*, 2022, **983**, 1–41.

21 G. Croft and M. J. Fuller, *Nature*, 1977, **269**, 585–586.

22 X. Wang, J. S. Tian, Y. H. Zheng, X. L. Xu, W. M. Liu and X. Z. Fang, *ChemCatChem*, 2014, **6**, 1604–1611.

23 X. Xu, X. Wang, Y. Li, J. Tian, W. Liu and Z. Gao, *Z. Phys. Chem.*, 2014, **228**, 27–48.

24 X. Xu, X. Sun, H. Han, H. Peng, W. Liu, X. Peng, X. Wang and X. Yang, *Appl. Surf. Sci.*, 2015, **355**, 1254–1260.

25 Y. Liu, Y. Guo, H. Peng, X. Xu, Y. Wu, C. Peng, N. Zhang and X. Wang, *Appl. Catal., A*, 2016, **525**, 204–214.

26 J. Choi, L. Pan, V. Mehar, F. Zhang, A. Asthagiri and J. F. Weaver, *Surf. Sci.*, 2016, **650**, 203–209.

27 C. Zhang, Y. Li, Y. Wang and H. He, *Environ. Sci. Technol.*, 2014, **48**, 5816–5822.

28 X. Sun, X. Peng, X. Xu, H. Jin, H. Wang and X. Wang, *J. Mol. Model.*, 2016, **22**, 204.

29 R. Ruus, A. Saar, J. Aark, A. Aidla, T. Uustare and A. Kikas, *J. Electron Spectrosc. Relat. Phenom.*, 1998, **93**, 193–199.

30 S. Salimian and M. Delfino, *J. Appl. Phys.*, 1991, **70**, 3970–3972.

31 X. Li, X. Sun, X. Xu, W. Liu, H. Peng, X. Fang, H. Wang and X. Wang, *Appl. Surf. Sci.*, 2017, **401**, 49–56.